Susceptibility of Static Energy Meters due to Amplifier Clipping Caused by a Rogowski Coil

Tom Hartman, *Member, IEEE*, Bas ten Have, *Member, IEEE*, Johan Dijkstra, Roelof Grootjans, *Member, IEEE*, Niek Moonen, *Member, IEEE*, and Frank Leferink, *Fellow, IEEE*

***Abstract*—Static energy meters installed in households, used for billing purposes of the energy consumption, have shown errors due to conducted electromagnetic interference coming from appliances in household situations. This resulted in over- and underestimations of the energy bill, and even in a perceived energy generation. The currents causing interference are known to be nonlinear pulsed currents with fast slopes. This article shows that clipping of the amplifier, following the Rogowski coil, which is used as the current sensing element, results in distorted energy measurements. Due to the pulsed nature of the current, the output of the Rogowski coil exceeds the maximum input voltage of the amplifier, resulting in clipping at the output of the amplifier. This clipped signal is then integrated in the digital chain, resulting in an offset in the perceived current. Hence, causing a higher or lower energy calculation, depending on the phase firing angle and the fastest edge of the pulse. It is found that parameters, such as the slew rate, rise and fall times, and firing angle, are correlated to the interference on static energy meters.**

***Index Terms*—Amplifier, clipping, conducted, electromagnetic interference (EMI), nonlinear equipment, phase firing angle, pulsed currents, Rogowski coil, static energy meter (SM).**

I. Introduction

In THE last decades, the use of nonlinear equipment, such as switched mode power supplies, has increased, as these are often more energy efficient [1]. However, this nonlinear equipment is creating more conducted electromagnetic interference (EMI) problems, especially in the frequency range from dc to 150 kHz, due to the lack of civil standards in this frequency range [2]. As a result, interference problems with static energy meters (SMs) were reported, where SMs measure the energy consumption of households for billing purposes [3]. The interference problems were, for instance, due to harmonic disturbances [4], photovoltaic installations [5], and power drive systems [6], which possibly combined with a higher number of complaints and failures, resulted in faster publication of the technical report CLC/TR50579 [7] and IEC 61000-4-19 Standard [8]. Afterward, more problems were observed by consumers, and investigations of these cases showed metering errors resulting from dimmed light-emitting diode and compact fluorescent lamps [9]. The performance of SMs in households was considered in [10] by including various harmonic voltages and currents, showing metering errors up to 25%. Furthermore, the largest errors observed in a household situation were due to a commercial off-the-shelf (COTS) speed controlled water pump [11]. This research reported serious erroneous overestimations of up to 2675%. The latest unanticipated finding came after a complaint of a consumer, where switching multimedia equipment presented a situation where a power generation of more than 600 W was measured by the SM. This occurred in a household while no power generating devices were installed and 25 W was actually being consumed by the load [12]. Over- and underestimations have been observed previously, but a perceived energy generation was unprecedented.

Most research on the interference on SMs, up until this point, has been performed by considering the SM as a black box, where at most the current transducer was known. However, the currents from COTS equipment causing EMI problems with SMs have been researched in the time domain, and are mostly nonlinear and have a pulsed shape [13]. A higher crest factor, narrower pulsewidth, less charge, firing angle (FA), and a faster slew rate (SR) were identified as the factors that contribute the most to the interference, and thus the faulty energy bills. However, the full relation between specific parameters of the waveforms and a root cause inside the SM resulting in these measurement errors remained unknown in previous publications. This is due to the COTS equipment used for testing, found via on-site cases in households, drawing a limited number of fixed waveforms. Furthermore, within this set of waveforms, there is no direct control over changing individual parameters. To overcome this problem, an ac controlled-current load has been designed and built to have full control over the waveforms being drawn, and the corresponding parameters [14]. The current inside an SM is measured using either a Rogowski coil, current transformer, Hall effect sensor, or shunt resistor. Rogowski coil meters, which are presently installed in many households due to their lower cost, are most susceptible to the highest metering errors of up to 2675%, as well as to the erroneous perceived energy

Manuscript received 28 June 2022; accepted 8 August 2022. Date of publication 26 September 2022; date of current version 14 December 2022. This work was supported by EMPIR Programme through Participating States and European Union's Horizon 2020 research and innovation programme under Project 17NRM02 MeterEMI. *(Corresponding author: Tom Hartman.)*

Tom Hartman, Bas ten Have, Johan Dijkstra, Roelof Grootjans, and Niek Moonen are with the University of Twente, 7522 NB Enschede, The Netherlands (e-mail: tom.hartman@utwente.nl; bas.tenhave@utwente.nl; j.k.dijkstra@student.utwente.nl; r.grootjans@utwente.nl; d.j.g.moonen@utwente.nl).

Frank Leferink is with the University of Twente, 7522 NB Enschede, The Netherlands, and also with the THALES Nederland B.V., 7554 RR Hengelo, The Netherlands (e-mail: leferink@ieee.org).

Color versions of one or more figures in this article are available at https://doi.org/10.1109/TEMC.2022.3204391.

Digital Object Identifier 10.1109/TEMC.2022.3204391

generation. This is related to the output of the Rogowski coil being proportional to the time derivative of the current in a combination with the drawn pulsed current. Current transformers and Hall effect sensors also cause errors, but in a smaller extent of up to a maximum of around 200%, while no significant errors occur with shunt resistors. Even though shunt resistors result in no significant errors, the fact remains that many susceptible SMs utilizing a Rogowski coil are still installed in households due to their lower cost.

Therefore, this article investigates the root cause for the susceptibility of SMs utilizing a Rogowski coil as their current transducer. The effect of the SR, rise and fall times, and phase FA of controlled pulsed currents on the erroneous energy measurements is analyzed. A fast SR creates a higher signal amplitude at the input of the signal amplifier due to the time-derivative effect of the Rogowski coil. These signals within the measurement chain of the SM are then mathematically described after which these relations are validated via simulations and measurements with SMs representing part of the installed base in Europe.

The rest of this article is organized as follows. Section II displays previous findings and describes the resulting hypothesis that explains the found errors on SMs utilizing a Rogowski coil as their current transducer. This is then further investigated via mathematical relations between specific waveform parameters and the measurement errors in Section III. Section IV shows the ac controlled-current load that is used and elaborates on the test signals used for the results. In Section V, the ac controlled-current load is used to reliably quantify SM errors and validate the hypothesis via simplified triangular current pulses making controlled changes to the loading conditions. This is followed up by the discussion in Section VI. Finally, Section VII concludes this article.

II. Analysis of a Static Energy Meter

This section shows an explanation how nonlinear currents cause clipping of the amplifier inside an SM and, thus, lead to erroneous energy measurements.

A. Previous Findings

Waveforms found to interfere most with the energy measurements of SMs are known to be of a pulsed nature, mostly caused by dimmers. This pulsed nature can be described by various parameters of interest, such as the SR, rise and fall times, crest factor (CF), and peak current. The critical range for the SR of an interfering pulse on SMs is identified from empirical data as being faster than 0.1 A/μs [13]. This also holds for the waveform known to cause the peculiar perceived energy generation, as seen in Fig. 1 [12]. This waveform is the result of a combination of COTS equipment encountered in a household situation, which draws pulsed currents with an SR of 2.5 A/μs at variable FAs. A variable FA, and the rising edge SR of this waveform being significantly faster than the falling edge SR, is due to the leading edge dimmer used. This situation was encountered in a household with an SM that utilizes a Rogowski coil as its current transducer. The equipment causes massive errors on the SM, ranging from a perceived power generation of more than 600 W at an FA of 45° to a perceived power consumption of more than 600 W at an FA of 135°, while in both cases, 25 W is actually being consumed.

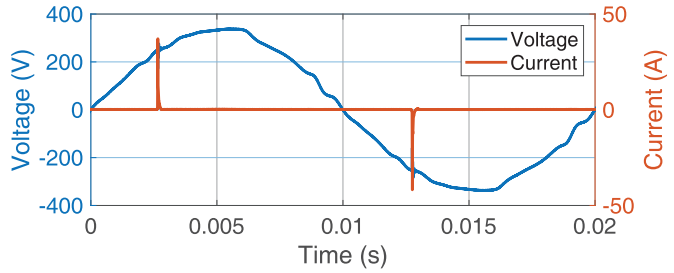

Fig. 1. Pulsed current drawn at an FA of 45° [12].

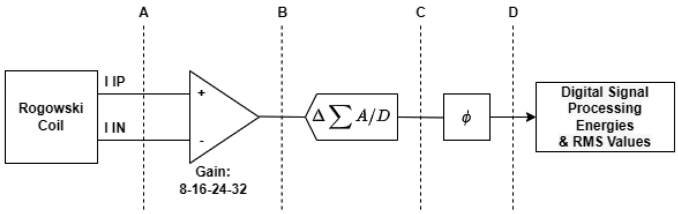

Fig. 2. Block diagram of the current measurement chain inside the STPM01 chip that is used in SMs [15].

TABLE I
Maximum Input Voltage of the Voltage and Current Channels of the Amplifier Inside an SM Giving Rise to Errors [15]

Voltage channels		Current channels	
Gain	Max input voltage (V)	Gain	Max input voltage (V)
4	±0.30	8×	±0.15
		16×	±0.075
		24×	±0.05
		32×	±0.035

B. Inside a Static Energy Meter

An energy metering IC known to be used inside SMs that utilize a Rogowski coil, installed in households in Europe, is the STPM01 chip [15]. A schematic overview of the current measuring chain inside an SM utilizing a Rogowski coil can be seen in Fig. 2. Inside the SM, the current is first measured via a Rogowski coil that differentiates the signal. The output of the Rogowski coil is then amplified and digitized when it enters the IC after which the phase error is calibrated for. Subsequently, the digital waveform is numerically integrated via digital signal processing to obtain the original current waveform.

A current waveform with a high SR will result in a relatively high amplitude at the output of the Rogowski coil, measured at point A of Fig. 2. This output of the Rogowski coil inside an SM, as a result of the waveform in Fig. 1, can be seen in Fig. 3(a), where the output of the Rogowski coil goes up to 1 V. This waveform is then amplified inside the chip for which the maximum input voltage of this amplifier is given in Table I. For all gain settings, the measured input voltage of 1 V at point A exceeds the limits of the amplifier inside the chip. Such a current waveform will, thus, always result in the clipping of the signal

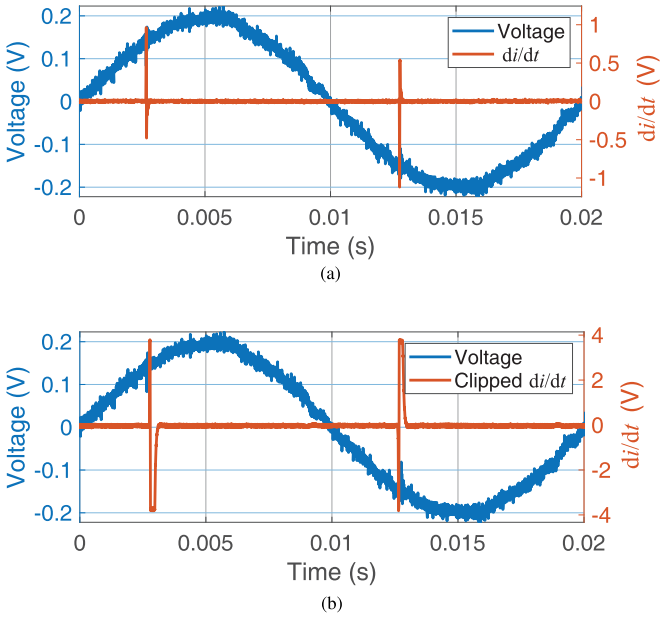

Fig. 3. Effect that a pulsed current with a high $\frac{di}{dt}$ has on the amplifier. (a) Output of the Rogowski coil measured inside the SM. (b) Clipped output of the amplifier.

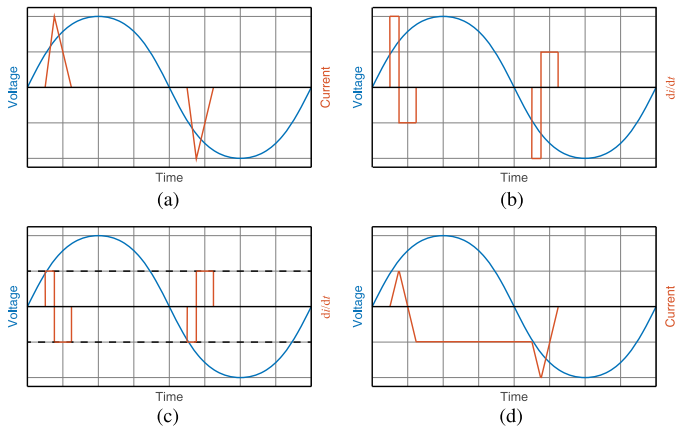

Fig. 4. Schematic overview of the clipping of the differentiated current. (a) Pulse with a fast rising edge. (b) Differentiated Rogowski coil output. (c) Clipped amplifier output. (d) Distorted current after integration.

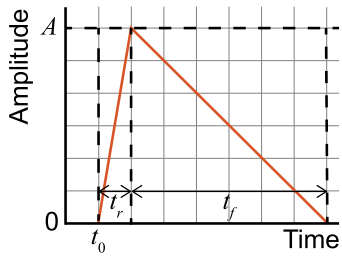

Fig. 5. Triangular pulsed waveform.

at the output of the amplifier, point B inside the SM. Since the amplifier inside an SM is incorporated inside the STPM01 chip, the output cannot be measured directly. However, to visualize the effect of clipping, an amplifier has been implemented with a maximum input voltage of 0.037 V, closely relating to the worst case scenario for the amplifier in Table I. The resulting clipped output can be seen in Fig. 3(b). For such a maximum input voltage, both the differentiated rising edge and falling edge of the pulse are clipped. However, in the case of Fig. 3, the rising edge was faster, and a larger portion of the differentiated rising part is clipped.

C. Clipping of the Amplifier

The clipping of the amplifier results in a distorted current waveform after numerically integrating the output of the amplifier, due to the difference in steepness of the rising edge and falling edge. This effect is shown in Fig. 4. A triangular pulse with a faster rising edge than the falling edge is chosen, which represents a simplified pulsed current [12], [13], which can be seen in Fig. 4(a). This signal is then differentiated via the Rogowski coil resulting in a higher output for the rising edge and a smaller negative value for the falling edge, see Fig. 4(b). Since the triangular current pulse started off at zero and returns to zero, the areas underneath the positive and negative slopes of the differentiated signal should be equal. However, this signal is then clipped by the amplifier resulting in a mismatch of the positive and negative areas, see Fig. 4(c). The positive $\frac{di}{dt}$ gets clipped resulting in a mismatch of areas and, thus, results in a distorted current waveform after integration, see Fig. 4(d). Due to the positive $\frac{di}{dt}$ being clipped, the resulting current waveform gets an unexpected negative offset. Multiplying this distorted current with the correctly measured voltage will then result in errors for SMs, which explains the case where a perceived energy generation is measured while energy is actually being consumed [12]. Solving the clipping of the amplifier, by increasing the maximum input voltage, or by placing a limiter, in combination with a detector, in front of the amplifier, would resolve SM errors that utilize Rogowski coils. Another solution is decreasing the slope of the current waveform, thus lowering the amplitude of the Rogowski coil output, which could be realized via a low-pass filter, as proposed in [16]. A third solution would be to use a passive integrator between the Rogowski coil and the amplifier, which is analogous to a low-pass filter.

III. Waveform Parameters Causing Errors

This section follows up on the susceptibility of SMs as a result of the amplifier clipping. A mathematical relation between the measurement error of SMs and the SRs, rise and fall times, and peak amplitude is given. The effect which the FA has on the error is shown via simulations.

A. Mathematical Description

A simplified triangular pulsed waveform with a constant SR over the rising edge and a constant SR over the falling edge, as is visualized in Fig. 5, is chosen as an approximation of a fast pulse for this analysis.

With a maximum amplitude defined as A, a rise time t_r and a fall time t_f are defined as the time difference between 0% and

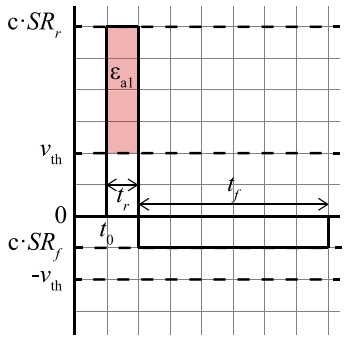

Fig. 6. High rising edge SR causing clipping in the rising edge.

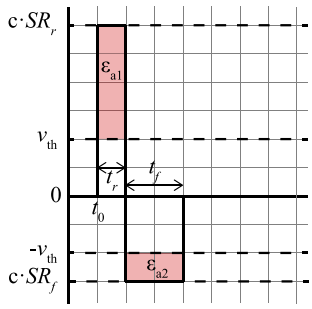

Fig. 7. High rising edge SR and falling edge SR causing clipping for both edges.

100% of the maximum amplitude. If such a pulsed waveform is measured by a Rogowski coil, its response is the differentiated current, for which the amplitude of the output is proportional to the SR, defined as SR_x as follows:

$$\mathrm{SR}_x = \frac{\Delta A}{t_x} \tag{1}$$

where x being either r or f, indicating the rising or falling edge, respectively, and ΔA being the change in amplitude. It is known that for such a simplified triangular pulsed waveform, the ideal output of the Rogowski coil looks like Fig. 6, where a significantly faster rising edge is chosen, based on waveforms known to produce errors. This causes the output of the Rogowski coil to be higher than the maximum input voltage of the amplifier, expressed as V_{th}. The proportionality of the output of the Rogowski coil to SR is indicated with $c \cdot \mathrm{SR}_r$ and $c \cdot \mathrm{SR}_f$ for the rising and falling edge, respectively.

Without clipping, the area under the graph always adds up to 0, meaning that the current rises with the same amplitude as it falls and resulting in no offset in the resulting current waveform after integration. The integration is written as follows:

$$\int_{t_0}^{t_0+t_r} c \cdot \mathrm{SR}_r \, dt + \int_{t_0+t_r}^{t_0+t_r+t_f} c \cdot \mathrm{SR}_f \, dt \tag{2}$$

thus resulting in the following:

$$c \cdot \mathrm{SR}_r \cdot t_r + c \cdot \mathrm{SR}_f \cdot t_f = c \cdot A + c \cdot -A = 0 \tag{3}$$

Due to the definition of the triangular pulsed waveform, (1), $\mathrm{SR}_r \cdot t_r = A$ and $\mathrm{SR}_f \cdot t_f = -A$. The red area ϵ_{a_1} in Fig. 6 represents the clipped positive area, causing a mismatch between the two areas and results in an erroneous negative offset in the current waveform after integrating the output of the amplifier. The calculation of the red area ϵ_{a_1} follows from the parameters in Fig. 6 and is given as follows:

$$\epsilon_{a_1} = t_r(c \cdot \mathrm{SR}_r - V_{\mathrm{th}}) \tag{4}$$

where c corresponds to the proportionality of the output of the Rogowski coil to the SR and where the equation only holds if $|c \cdot \mathrm{SR}_r| \geq V_{\mathrm{th}}$. The area ϵ_{a_1} can be described by the variables of the current waveform, shown in Fig. 5, and the maximum input voltage of the amplifier, defined as V_{th}, by combining (4) and (1), which results in the following:

$$\epsilon_{a_1} = c \cdot A - t_r \cdot V_{\mathrm{th}}. \tag{5}$$

Equation (5) shows that an increase in amplitude linearly increases the erroneous area. If the rise and fall times are kept constant, this results in an increase of both the rising and falling SR. This increase in SR could also cause the falling edge output of the Rogowski coil to exceed $-V_{\mathrm{th}}$, resulting in a negative area that also gets clipped. For this reason a faster falling edge is assumed in Fig. 7 when compared with the previous pulse. This negative area ϵ_{a_2} is also subtracted, thus reducing the negative offset resulting from ϵ_{a_1}.

The effective area causing the resulting offset in the current is defined as follows:

$$\epsilon_a = \epsilon_{a_1} + \epsilon_{a_2} = t_r(c \cdot \mathrm{SR}_r - V_{\mathrm{th}}) + t_f(c \cdot \mathrm{SR}_f + V_{\mathrm{th}}) \tag{6}$$

$$= c \cdot A - t_r \cdot V_{\mathrm{th}} + -c \cdot A + t_f \cdot V_{\mathrm{th}} \tag{7}$$

where ϵ_{a_1} was already defined in (5), and ϵ_{a_2} is defined as a negative area in the following:

$$\epsilon_{a_2} = t_f(c \cdot \mathrm{SR}_f + V_{\mathrm{th}}) = -c \cdot A + t_f \cdot V_{\mathrm{th}}. \tag{8}$$

In (7), $\epsilon_{a_x} = 0$ if $|c \cdot \mathrm{SR}_x| \leq V_{\mathrm{th}}$. If $|\epsilon_{a_1}| > |\epsilon_{a_2}|$, a positive area is clipped, resulting in a negative offset in the current. Vice versa, when $|\epsilon_{a_1}| < |\epsilon_{a_2}|$, a negative area is clipped, thus resulting in a positive offset in the resulting current. This shows that the fastest edge, rising or falling, determines the polarity of the erroneous offset introduced in the current.

The mathematical relations in this section show the influence of the waveform parameters seen in (1) on the SM error. Using these three waveform parameters, the mathematical relations will be validated with measurements via three different situations in Section V. This is done by constantly keeping one of the three parameters constant, while changing the other two.

B. Simulation

In this section, the theoretical approach will be further elaborated on via simulations in MATLAB. This is done to validate the effect that the FA of a pulsed current has on SM errors. Resulting in either a perceived, much higher, energy generation for a drawn current at an FA below 90°, while also showing a perceived, much higher, energy consumption for the same drawn current at an FA between 90° and 180° [12]. The same type of pulsed current signal, as discussed in Section III-A, is used, with a faster rising edge compared with the falling edge. For the simulations in this section, all the current waveforms have been normalized to 1.

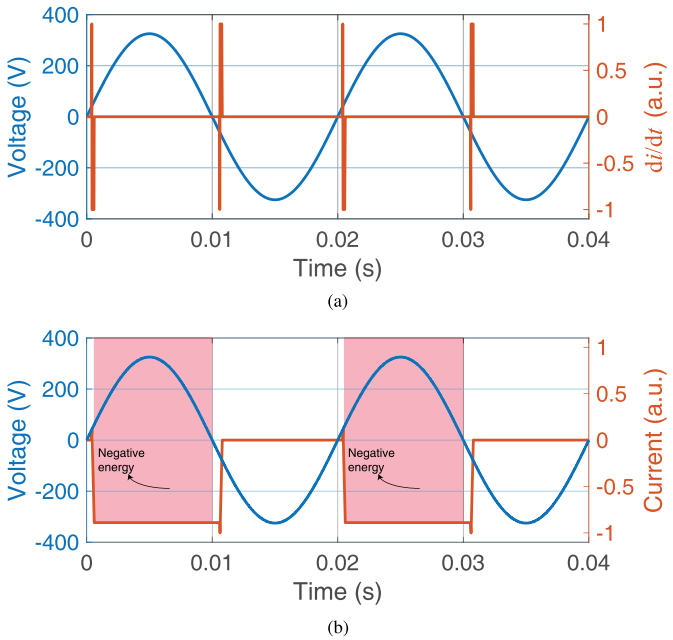

Fig. 8. Clipped amplified differentiated current with (a) an FA of 5° and (b) the resulting negative offset in the current. (a) Normalized clipped amplifier output of a pulse with a FA of 5°. (b) Normalized current after integrating a pulse with a FA of 5°.

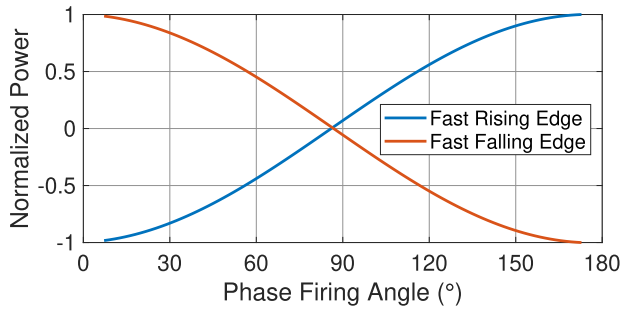

Fig. 9. Normalized power for all FAs for the resulting offsets in the currents.

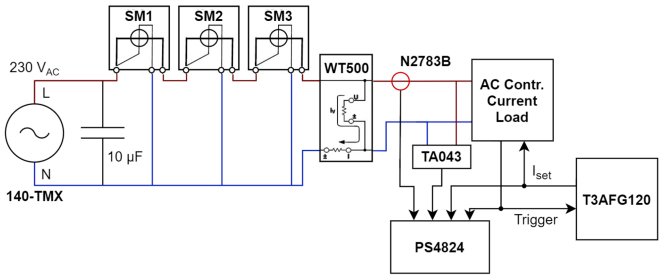

Fig. 10. Schematic overview of the measurement setup used.

In Fig. 8(a), such a clipped output of the amplifier signal is plotted for an FA of 5°. Due to the higher positive part and the lower negative part being clipped both toward the same value, a distorted current signal will be reproduced when integrating this distorted signal. The result of this integration can be seen in Fig. 8(b), where a negative offset in the current signal arises between the two pulses in one full cycle due to the longer in time, equal in value, negative $\frac{di}{dt}$ with respect to the short positive $\frac{di}{dt}$.

If this distorted current signal is used for the power calculation, it is clear that this will result in a negative power value, and thus a perceived higher power generation.

However, if the FA of the pulse is shifted with respect to the voltage, the same effect results in a different error. The same type of distorted current, but with an erroneous offset starting at an FA of 90° and stopping at 270°, will in this case result in a perceived net-zero error. This is due to the positive and negative parts around the zero-crossing of the voltage cancelling out when multiplied with the negative offset around this zero-crossing. Following the same logic, an erroneous offset starting at an FA around 175° will result in a higher perceived energy consumption due to the negative offset being multiplied by the negative voltage. These three cases explain the effect the FA of a current pulse has on the errors of SMs utilizing a Rogowski coil, explicitly identified in [12].

The average power calculations with the negative offset in the current for all possible FAs between 5° and 175° have been carried out and normalized. The results can be seen with the blue line in Fig. 9, where it is clearly seen that for these type of triangular pulses, the power goes from a maximum worst case power generation around 5° toward a maximum worst case power consumption at 175°. From these results and (7), the exact opposite graph is expected when looking at triangular pulses with a falling edge that is significantly faster than the rising edge shown with the red line in Fig. 9. This type of current pulse, with a slow rising edge and fast falling edge, and thus a resulting error, has not been detected with a real COTS appliance. However, the effect of such a current on SM errors will be validated in Section V, since trailing edge dimmers could bring about such waveforms. From these simulations and (7), four cases can be distinguished and the following hypothesis can be made:

1) fast rising edges below 90° will result in a negative error,
2) fast falling edges below 90° will result in a positive error,
3) fast rising edges between 90° and 180° will result in a positive error,
4) fast falling edges between 90° and 180° will result a negative error.

IV. AC Controlled-Current Load

This section describes the measurement setup used to adjust waveform parameters in a controllable manner, such that the theoretical analysis and simulations can be validated. The test signals are defined to portray the different distorted scenarios of Section III and are, thus, double-exponential pulses, representing a real life case of the simplified triangular pulse shape.

A. Measurement Setup

To verify the cause of erroneous readings of SMs utilizing a Rogowski coil, the measurement setup shown in Fig. 10 has been realized. The ac controlled-current load is able to draw arbitrary currents, which enables the testing of SMs in a controllable manner by adjusting current waveform parameters. A waveform generator (Teledyne T3AFG) is used to regulate the current

TABLE II
WAVEFORM CHARACTERISTICS

	t_r	t_f	Peak	Rising SR	Falling SR	FA
S1	10 µs	500 µs	5 A	0.5 A/µs	-0.01 A/µs	45 °
S2	500 µs	10 µs	5 A	0.01 A/µs	-0.5 A/µs	45 °
S3	10 µs	500 µs	5 A	0.5 A/µs	-0.01 A/µs	135 °
S4	500 µs	10 µs	5 A	0.01 A/µs	-0.5 A/µs	135 °

waveforms which the ac controlled-current load will draw from the ac voltage source. Furthermore, the load generates a pulse every zero-crossing to synchronize the current waveform with the voltage. The source voltage is generated using the Pacific Power Smart Source 140-TMX, which is a four-quadrant ac voltage source. In order to prevent the instability of the ac load and to reduce voltage transients during a fast SR, a 10 μF capacitor has been added to reduce the impedance seen by the load and allow for faster current pulses [17]. The 10 μF represents all C_x capacitors used in the power systems, and is based on the 10 μF as used in various standards (AECTP501 and MIL-STD 461G). This capacitor has been added in front of the SMs, such that the reactive current will not flow through these meters. Three SMs have been added in the setup, of which SM2 and SM3 have a Rogowski coil to measure the current. SM1 is used as a control SM, which uses a current transformer to measure the current. All the individual consumption of the SMs have been compensated for in the results. Furthermore, a Yokogawa WT500 power analyzer, with a power accuracy of 0.1%, is used as the reference for the actual consumed power, which is used in the calculation of the error. The voltage and current waveforms are captured using an oscilloscope (PicoScope PS4824) with a 20 MHz bandwidth sampling at 5 MHz. The voltage is measured using a Pico Technology TA043 differential voltage probe and the current is measured with a Keysight N2783B current probe, both with a bandwidth of 100 MHz. The current waveforms can be drawn in a controllable manner using this setup, which was not possible with COTS equipment. Parameters of the test waveforms can be adjusted in such a way that a relationship can be found between one, or interconnected, parameter(s) and SM errors.

B. Test Signals

A reference waveform S1 will be used as the basic waveform. Parameters of this waveform, such as the rise time, fall time, FA, SRs, and peak amplitude, will be changed in a controllable manner. The characteristics of the reference waveform S1 together with flipped and phase-shifted versions, S2, S3, and S4, can be seen in Table II. These four waveforms were chosen due to findings in previous research, showing the difference between leading edge and trailing edge dimming [11], [12], [18]. The resulting waveforms can be seen plotted together in Fig. 11, where the voltage is plotted as a reference for the phase differences. Since we can fully control the approximated triangular pulses, the rise and fall times used in this article are defined as the time from 0% to 100% of the peak amplitude of the signal, such that together they form the full width of the pulse.

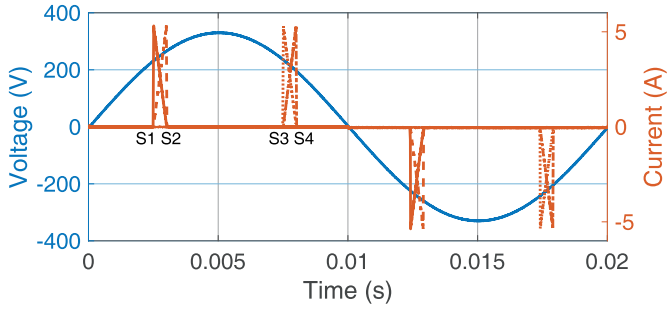

Fig. 11. Reference triangular pulse S1, together with S2, S3, and S4.

TABLE III
WAVEFORM ERRORS

	SM1	SM2	SM3	Reference	ΔSM2	ΔSM3
S1	35 W	-28 W	-32 W	35 W	-63 W	-67 W
S2	36 W	+80 W	+80 W	37 W	+43 W	+43 W
S3	33 W	+91 W	+92 W	33 W	+58 W	+59 W
S4	31 W	-22 W	-25 W	32 W	-54 W	-57 W

S2 is a flipped version of S1, where the rise and fall times are switched. S3 is a phase-shifted version of S1, while S4 also has the same phase shift as S3, but is again flipped. Following the hypothesis at the end of Section III, the following predictions can be made:

1) *S1:* negative error (generation) [12], [18],
2) *S2:* positive error (consumption) [18],
3) *S3:* positive error (consumption) [11], [12], [18],
4) *S4:* negative error (generation) [18].

V. RESULTS

Individual parameters of the approximated pulsed triangular waveforms are changed per section and a resulting change in errors of the SMs will be shown. First the effect of the rising edge versus the falling edge is shown to represent leading edge dimmers versus trailing edge dimmers. This is followed by the effect the FA has on the error. Then, the effect of the three waveform parameters from (1) on the SM error is demonstrated in three individual sections.

A. Rising Edge Versus Falling Edge

The four waveforms from Fig. 11 are tested individually on the SMs together with the reference power analyzer. The results can be seen in Table III, where ΔSM2 and ΔSM3 are the errors in watts between the SMs and the reference power analyzer. The difference, ΔSM1, between SM1 and the reference power analyzer is not in the table since this SM shows no significant errors. From the results in Table III, it is found that all four predictions according to the hypothesis are correct. Only a minor difference in magnitude between the different waveforms can be seen.

B. Phase Firing Angle

In this section, S1 is used as the reference waveform. For this section, the FA is changed between the different measurements,

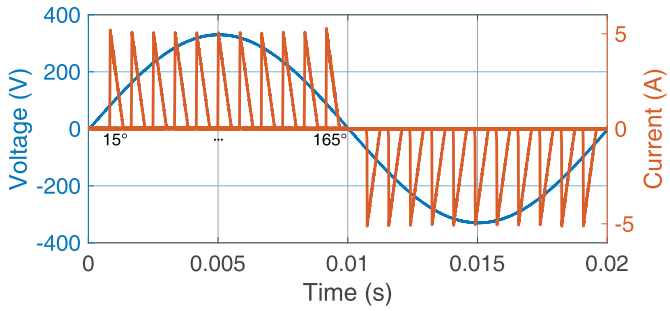

Fig. 12. Eleven triangular pulses at different FAs.

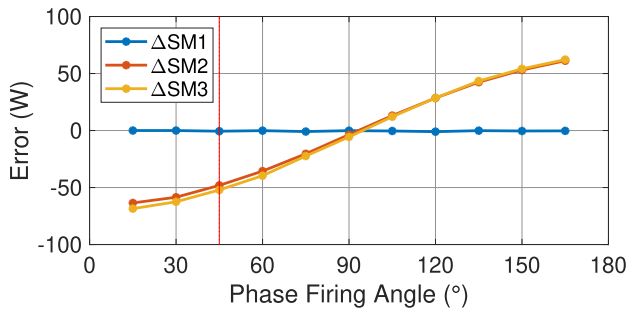

Fig. 13. SM errors for different FAs.

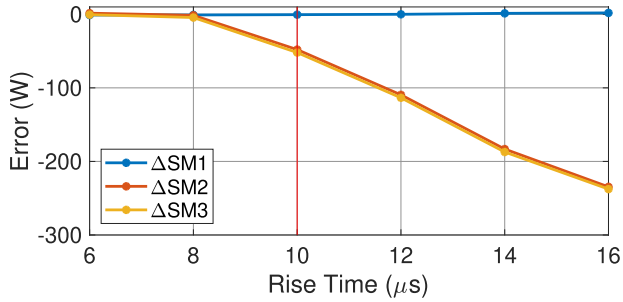

Fig. 14. SM errors for different rise times with a constant SR.

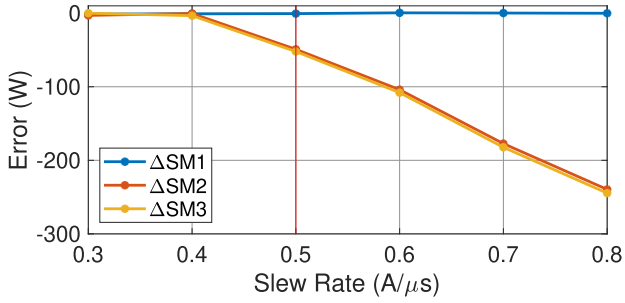

Fig. 15. SM errors for different SRs with a constant rise time.

while keeping the rise time, SR, and peak amplitude constant. The FA is changed from 15° to 165° in steps of 15°. The corresponding 11 waveforms can be seen plotted together in Fig. 12.

All 11 waveforms have been tested individually and the resulting differences between the SMs and the reference power analyzer can be seen in Fig. 13. S1 is indicated by the vertical red line, and will be indicated in all following figures showing SM errors. No significant error can be seen for SM1, while SM2 and SM3 show the same curve, as predicted in Fig. 9. An offset can be seen between SM2 and SM3 for negative errors, while this offset goes away for positive errors.

C. Constant Slew Rate—Increasing Rise Time

S1 is used again as the reference current waveform, for which the rise time is changed, while keeping the SR_r constant, thus also changing the peak amplitude, following (1). For all results shown hereafter, unless stated otherwise, the fall time is chosen such that $|c \cdot \mathrm{SR}_f| \leq V_{\mathrm{th}}$, resulting in (8) to equal zero, while $|c \cdot \mathrm{SR}_r| \geq V_{\mathrm{th}}$. The FA will also be kept constant for the following cases. From (4) it is seen that increasing t_r while keeping SR_r constant will increase the clipped area, and thus increase the negative offset resulting in a bigger error. The resulting errors for different waveforms with rise times ranging from 6 until 16 μs and peak amplitudes ranging from 3 to 8 A are plotted in Fig. 14. For waveforms with rise times below 8 μs, no significant errors can be found with an SR of 0.5 A/μs. Rise times higher than 8 μs show a linear increase in error when increasing the amplitude while keeping the SR constant, following (4).

D. Constant Rise Time—Increasing Slew Rate

In this section, SR_r of S1 is changed, while keeping the rise time constant, thus also changing the amplitude with it. From (4), it follows that this results in a linear increase of the error. SR_r is increased from 0.3 to 0.8 A/μs, and thus also increasing the peak amplitude from 3 to 8 A. The resulting SM errors are plotted against the different values for SR_r in Fig. 15.

E. Constant Peak Amplitude—Increasing Slew Rate

1) Rising Edge: In this section, several measurements were performed while increasing the SR_r, but keeping the peak amplitude constant, thus decreasing the rise time. In total, ten SR_r values, ranging in a logarithmic scale between 0.01 and 2 A/μs, are used. From (5) it is seen that decreasing t_r toward zero, as a result of increasing SR_r, while keeping A constant increases the area toward a maximum of $c \cdot A$. The resulting errors can be seen in Fig. 16, where no errors can be seen for an SR_r below 0.1 A/μs, for all three SMs. After this value for the SR_r, the errors start increasing as the SR_r increases up to 1 A/μs. From that point, the increase in error reduces while further increasing the SR_r.

2) Falling Edge: From (7) it was shown that increasing the SR_f would counteract the negative offset arising from ϵ_{a_1} if $|c \cdot \mathrm{SR}_f| \geq V_{\mathrm{th}}$. For this reason this section looks at the effect of decreasing the fall time, as a result of increasing the SR_f, while keeping the amplitude constant, getting the falling edge above the voltage threshold. Again the logarithmic scaling between 0.01 and 2 A/μs is used, where the SR_f of 0.01 A/μs corresponds to S1. The SR_f is then increased, and the resulting errors can be seen in Fig. 17. In Fig. 17, it can, indeed, be seen that increasing

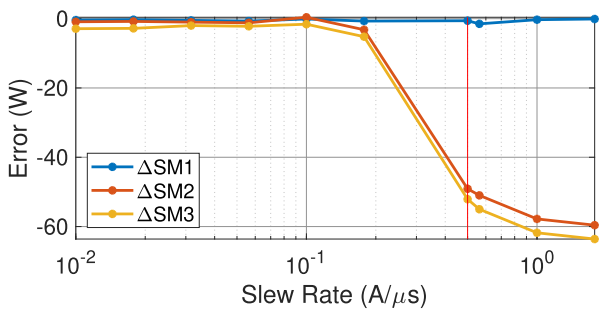

Fig. 16. SM errors for different rising edge SRs with a constant peak amplitude.

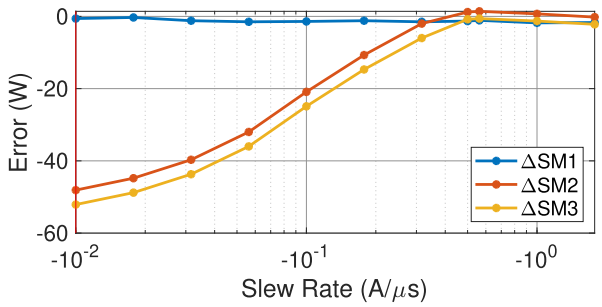

Fig. 17. SM errors for different falling edge SRs with a constant peak amplitude.

the SR_f up to the SR_r decreases the error and cancels out the clipping effects.

VI. Discussion

From the measurements performed in Section V, the effect that waveform parameters, such as SR, rise and fall times, and FA, have on the SM errors has been validated. Due to integration of the signal occurring after the clipping of the amplifier, the magnitude of the erroneous measurements of SMs utilizing a Rogowski coil is the most extreme with respect to SMs utilizing other current transducers. SMs that utilize a Rogowski coil, in their current state, will remain susceptible to conducted EMI and even more so in the future electronic environment of a household, with the continuous increasing use of non-linear equipment. If the robustness of SMs is not improved, more EMI problems will occur, resulting in more over- and underestimations of the energy bill of consumers. However, now that the underlying cause for the erroneous energy measurements is known, a solution can be implemented to prevent the errors in newer SM models. Possible solutions are: an increase of the maximum input voltage of the amplifier, placing a limiter in front of the amplifier, a low-pass filter behind the Rogowski coil, the use of a passive integrator, or changing the current sensing element. The question still remains if replacing the installed faulty meters with a more robust version is cost efficient, considering the installation costs or that SM errors can be tackled on a case to case basis. However, future meters still being installed should significantly improve on their robustness, especially the ones that utilize a Rogowski coil, which can be realized relatively low cost during the production process. The EMI problems with SMs once again show that properly considering electromagnetic compatibility (EMC) during the design process reduces the costs related to EMC significantly when compared with considering EMC in hindsight.

VII. Conclusion

A reason behind SMs, which utilize a Rogowski coil, being susceptible to interference has been examined. It was found that current waveforms with a high SR result in such high voltages at the output of the Rogowski coil that the amplifier will clip the signal. This clipping occurs because the maximum input voltage of the amplifier is exceeded. This results in a distorted current coming out of the numerical integrator, which has an offset introduced due to the clipping of the amplifier. A direct relation between parameters, such as the rise time, fall time, SRs and FA, and the corresponding SM errors, is given. All theoretical predictions have been confirmed by measurements on SMs, performed with a custom-built ac controlled-current load, capable of drawing custom current waveforms. A triangular pulse with a significantly faster rising edge with respect to the falling edge is considered as the reference pulse, such that the rising edge gets clipped in the amplifier while the falling edge does not. It was confirmed that phase shifting such an approximated triangular pulse flips the error from a negative power, thus a perceived power generation, below 90° to a positive error in power for a phase shift between 90° and 180°. Flipping the pulse itself, thus having a slow rising edge and a significantly faster falling edge, also flips the resulting errors. Furthermore, increasing the rise time while keeping the SR constant increases the error linearly, as does increasing the SR while keeping the rise time constant. Increasing the slower edge, the falling edge for the reference signal, up to the faster edge, counteracts the induced error. The theoretical and experimental results confirmed and explained many of the SM errors as observed in actual installations.

References

[1] M. Pourarab, S. Alishahi, and M. H. Sadeghi, "Analysis of harmonic distortion in distribution networks injected by nonlinear loads," in *Proc. 21st Int. Conf. Electricity Distrib.*, Frankfurt, Germany, 2011, pp. 1–4.

[2] K. Murakawa, N. Hirasawa, H. Ito, and Y. Ogura, "Electromagnetic interference examples of telecommunications system in the frequency range from 2 kHz to 150 kHz," in *Proc. Int. Symp. Electromagn. Compat.*, Tokyo, Japan, 2014, pp. 581–584.

[3] R. Masnicki, "Some remarks on the accuracy of energy meters," in *Proc. IEEE Int. Conf. Environ. Elect. Eng. IEEE Ind. Commercial Power Syst. Europe*, Palermo, Italy, 2018, pp. 1–5.

[4] A. Cataliotti, V. Cosentino, and S. Nuccio, "Static meters for the reactive energy in the presence of harmonics: An experimental metrological characterization," *IEEE Trans. Instrum. Meas.*, vol. 58, no. 8, pp. 2574–2579, Aug. 2009.

[5] J. Kirchhof and G. Klein, "EMV - Grenzwertlücke–Wechselrichter stört Zähler," in *Proc. 24th Symp. Photovoltaische Solarenergy*, Bad Staffelstein, Germany, 2009, pp. 1–8.

[6] P. Kotsampopoulos et al., "EMC issues in the interaction between smart meters and power-electronic interfaces," *IEEE Trans. Power Del.*, vol. 32, no. 2, pp. 822–831, Apr. 2017.

[7] *Electricity Metering Equipment - Severity Levels, Immunity Requirements and Test Methods for Conducted Disturbances in the Frequency Range 2–150 kHz*, CENELEC, Brussels, Belgium, Slovenski Standard CLC / TR 50579, 2012.

[8] *Electromagnetic Compatibility (EMC) - Part 4-19: Testing and Measurement Techniques - Test for Immunity to Conducted, Differential Mode Disturbances and Signalling in the Frequency Range From 2 Khz to 150 Khzat a.c. Power Ports*, IEC, Geneva, Switzerland, IEC Standard 61000-4-19, 2014.

[9] Z. Marais, H. E. Van den Brom, G. Rietveld, R. Van Leeuwen, D. Hoogenboom, and J. Rens, "Sensitivity of static energy meter reading errors to changes in non-sinusoidal load conditions," in *Proc. IEEE Int. Symp. Electromagn. Compat.- EMC EUROPE,*, Barcelona, Spain, 2019, pp. 202–207.

[10] J. R. Macedo Jr., G. L. Xavier, I. N. Gondin, L. T. S. Oliveira, and R. F. B. de Oliveira, "An update on the performance of active energy meters under non-sinusoidal conditions," *Elect. Eng.*, vol. 102, pp. 1785–1794, Apr. 2020.

[11] B. ten Have, T. Hartman, N. Moonen, C. Keyer, and F. Leferink, "Faulty readings of static energy meters caused by conducted electromagnetic interference from a water pump," *Renewable Energy Power Qual. J.*, vol. 17, no. 17, pp. 15–19, 2019.

[12] T. Hartman, B. ten Have, N. Moonen, and F. Leferink, "How to earn money with an EMI problem: Static energy meters running backwards," in *Proc. Joint IEEE Int. Symp. Electromagn. Compat., Signal Power Integrity, EMC Europe*, Glasgow, U.K., 2021, pp. 1–6.

[13] B. ten Have et al., "Waveform model to characterize time-domain pulses resulting in EMI on static energy meters," *IEEE Trans. Electromagn. Compat.*, vol. 63, no. 5, pp. 1542–1549, Oct. 2021.

[14] J. Dijkstra, T. Hartman, N. Moonen, and F. Leferink, "An ac controlled-current load for controllable waveform parameters to quantify static energy meter errors," in *Proc. IEEE Int. Symp. Electromagn. Compat. Signal/Power Integrity*, 2020, pp. 472–477.

[15] STMicroelectronics, "Programmable single phase energy metering IC with tamper detection," STMicroelectronics, Geneva, Switzerland, STPM01 Datasheet, Doc ID 10853 Rev 8, Jun. 2011.

[16] T. Hartman, R. Grootjans, N. Moonen, and F. Leferink, "Electromagnetic compatible energy measurements using the orthogonality of nonfundamental power components," *IEEE Trans. Electromagn. Compat.*, vol. 63, no. 2, pp. 598–605, Apr. 2021.

[17] E. Kaufhold, J. Meyer, S. Müller, and P. Schegner, "Probabilistic stability analysis for commercial low power inverters based on measured grid impedances," in *Proc. IEEE 9th Int. Conf. Power Energy Syst.*, 2019, pp. 1–6.

[18] T. Hartman, R. Grootjans, N. Moonen, and F. Leferink, "The effects of falling and rising edge dimming on static energy meter errors," in *Proc. IEEE Asia-Pacific Int. Symp. Electromagn. Compat.*, Bali, Indonesia, 2021, pp. 1–6.

Tom Hartman (Member, IEEE) received the bachelor and master degrees in electrical engineering in 2016 and 2018, respectively from the Group of Telecommunication Engineering, University of Twente, Enschede, The Netherlands, where he has been working toward the Ph.D. degree in electromagnetic compatibility with the Power Electronics and Electromagnetic Compatibility Group, since August 2018.

Since August 2021, he has been a Lecturer with the same group. Mr. Hartman was the recipient of the 2021 President Memorial Award of the IEEE EMC Society.

Bas ten Have (Member, IEEE) received the B.Sc. and M.Sc. degrees in electrical engineering in 2015 and 2018, respectively, from the University of Twente, Enschede, The Netherlands, where he has been working toward the Ph.D. degree in electromagnetic compatibility with the Power Electronics and Electromagnetic Compatibility Group, since June 2018.

His research interests include energy efficiency, innovations of products, systems and applications, low-frequency electromagnetic interference, power systems, power electronics, and smart grids.

Johan Dijkstra received the B.Sc. degree in electrical engineering in 2019 from the University of Twente, Enschede, The Netherlands, where he has been working toward the M.Sc. degree in electrical engineering with power electronics as specialization, since September 2021.

Since then, he has been with the Power Electronics and Electromagnetic Compatibility Group, where he developed an electronic load used to test static energy meters.

Roelof Grootjans (Member, IEEE) received the M.Sc. degree in 2016 in electrical engineering from the Telecommunications Group, University of Twente, Enschede, The Netherlands.

Since then, he has been with a small company that develops explosive trace detection equipment using ion mobility spectrometry. Since August 2019, he has been a Technician with the University of Twente to support lab activities and electronics development related to electromagnetic compatibility and power electronics.

Niek Moonen (Member, IEEE) received the B.Sc. degree in advanced technology, the M.Sc. degree in electrical engineering, and the Ph.D. (*cum laude*) degree in electromagnetic compatibility from the University of Twente, Enschede, The Netherlands, in 2012, 2014, and 2019, respectively.

Since January 2019, he has been with the Power Electronics and Electromagnetic Compatibility Group, University of Twente, first as a Senior Researcher and currently as an Assistant Professor. His research interests include electromagnetic interference (EMI) mitigation in power electronics with special interest in EMI propagation in smart grids, digital signal processing in electromagnetic compatibility measurements, and EMI filter optimization.

Dr. Moonen is a Member of the IEEE Electromagnetic Compatibility Society TC7 on low-frequency EMC and a Board Member of the Dutch EMC-ESD Association.

Frank Leferink (Fellow, IEEE) received the B.Sc., M.Sc., and Ph.D. degrees in electrical engineering from the University of Twente, Enschede, The Netherlands, in 1984, 1992, and 2001, respectively.

Since 1984, he has been with THALES, Hengelo, The Netherlands, and is currently the Director of EMC. He is also the Manager with the Network of Excellence on EMC, THALES Group, with more than 100 EMC engineers scattered over more than 20 units, worldwide. In 2003, he joined as (part-time, full research) Professor and holds the Chair for EMC with the University of Twente. He has authored or coauthored more than 300 papers published in international conferences or peer-reviewed journals, and he holds five patents.

Dr. Leferink is the Past President of the Dutch EMC-ESD Association, Chair of the IEEE EMC Benelux Chapter, Member of ISC EMC Europe, Chairman of EMC Europe 2018 (Amsterdam, The Netherlands), Member of the Board of Directors of the IEEE EMC Society, and Associate Editor for IEEE TRANSACTIONS ON ELECTROMAGNETIC COMPATIBILITY and IEEE LETTERS ON ELECTROMAGNETIC COMPATIBILITY PRACTICE AND APPLICATIONS.